Matrix Biology 31 (2012) 81–89

Contents lists available at SciVerse ScienceDirect

Matrix Biology

journal homepage: www.elsevier.com/locate/matbio

A comprehensive model of hyaluronan turnover in the mouse

Laurence Jadin *, Louis H. Bookbinder, Gregory I. Frost

Halozyme Therapeutics Inc., San Diego, CA, USA

ARTICLE INFO

Article history:
Received 11 May 2011
Received in revised form 3 November 2011
Accepted 14 November 2011

Keywords:
Hyaluronan
Hyaluronidase
Glycosaminoglycan
Pharmacokinetics
Turnover

ABSTRACT

The metabolism of hyaluronan (HA), especially its catabolism, is still far from being elucidated. Although several studies suggest that HA is degraded locally in tissues and through the lymphatic or circulatory systems, much needs to be learned about the enzymes, receptors and cell types that support this dynamic process. In the current work, the clearance of exogenously administered HA was examined in a C57BL/6 mouse model. Hyaluronidase-sensitive fluorescein-labeled 1.2 MDa hyaluronan (flHA) was administered either intravenously (i.v.) or subcutaneously (s.c.) into wild type C57BL/6 mice. Plasma was sampled for pharmacokinetic analysis and tissues were harvested for histological examination of the cell types responsible for uptake using immunofluorescent localization and for size exclusion chromatography analysis. We observed that flHA could be degraded locally in the skin or be taken up by sinusoidal cells in lymph nodes, liver and spleen. I.v. administration of flHA revealed non-linear Michaelis–Menten pharmacokinetics compatible with a saturable, receptor-mediated clearance system ($K_m = 11.6\ \mu g/ml \pm 46.0\%$, $V_{max} = 1.69\ \mu g/ml/min \pm 59.7\%$). Through a combination of immunofluorescence microscopy, pharmacokinetic, and chromatographic analyses of labeled substrate in vivo, our results shed additional light on the mechanisms by which HA is catabolized in mammals, and serve as a basis for future studies.

1. Introduction

The metabolism of hyaluronan (HA), a ubiquitous glycosaminoglycan of the extracellular matrix of vertebrates, is a source of increasing interest. HA-depolymerizing activity was associated with a spreading factor first identified in mammalian testis extracts in 1928 (Duran-Reynals, 1928), and HA biosynthesis by cell-free extracts of streptococci was demonstrated 30 years later (Markovitz et al., 1958). Multiple HA synthases and hyaluronidases have been identified and cloned from vertebrates as well as bacteria (DeAngelis et al., 1993; Itano and Kimata, 1996a; Itano and Kimata, 1996b; Watanabe and Yamaguchi, 1996; Frost et al., 1997; Spicer et al., 1997; Strobl et al., 1998). However, the catabolic pathways responsible for the clearance of HA from the total vertebrate body have not been adequately described.

HA is found in the extracellular matrix of most connective tissues as a polymer of N-acetylglucosamine and glucuronic acid that can reach several megadaltons in size. All HA synthases possess the two glycosyltransferase activities responsible for the transfer of UDP-N-acetylglucosamine and UDP-glucuronic acid during the synthesis of HA chains (DeAngelis and Weigel, 1994). Three different isoforms have been described in mammals that differ in terms of length and amount of HA they can produce (Itano et al., 1999). Several paralogous hyaluronidases have also been identified in mammalian genomes (Csoka et al., 1999; Csoka et al., 2001), but for the most part their precise role in HA catabolism remains unclear. The most commonly accepted model of somatic HA catabolism is a 2-step linear pathway occurring in certain types of cells involving hyaluronidases-1 and -2 (HYAL1 and HYAL2) (Csoka et al., 2001; Stern, 2003; Stern, 2004). According to this model, the glycosylphosphatidylinositol (GPI)-anchored HYAL2 initiates HA degradation at the plasma membrane in an acidified microenvironment (Bourguignon et al., 2004). Subsequently, HA is internalized by a receptor-mediated mechanism and travels through the endocytic pathway to reach the lysosomes where it is further degraded by HYAL1 and exoglycosidases to generate monosaccharide end-products. The fact that this model has not yet been validated in mammals is surprising considering the many important functions of HA, including its role in disease.

In the rabbit, whereas local turnover has been demonstrated in the skin (where half of the total HA resides), a significant part is removed by the lymph and taken up by the lymph nodes or by the liver after reaching the bloodstream (Laurent et al., 1991). Liver sinusoidal endothelial cells appear to play a role in the clearance of circulating HA (Smedsrod et al., 1990). Stabilin-2, (referenced in the present

Abbreviations: AUC, area under the curve; BSA, bovine serum albumin; CV, coefficient of variation; DMSO, dimethylsulfoxide; EDTA, ethylenediaminetetraacetic acid; flHA, fluorescein-labeled HA; GPI, glycosylphosphatidylinositol; HA, hyaluronan; HABP, hyaluronan binding protein; HARE, HA receptor for endocytosis; HYAL, hyaluronidase; MW, molecular weight; OCT, optimal cutting temperature; PBS, phosphate buffered saline; rHuPH20, recombinant human PH20; TAE, Tris-Acetate-EDTA; V, volt; *Vd*, volume of distribution; V_{max}, maximum elimination rate; i.v., intravenous; s.c., subcutaneous; SD, standard deviation.

* Corresponding author. Tel.: +1 858 704 8329.
E-mail address: ljadin@halozyme.com (L. Jadin).

0945-053X/$ – see front matter © 2011 Elsevier B.V. All rights reserved.
doi:10.1016/j.matbio.2011.11.002

work as HARE [HA receptor for endocytosis]), a scavenger receptor that binds and internalizes HA in vitro, is expressed on these and other sinusoidal cells and apparently supports the in vivo turnover of HA (Yannariello-Brown et al., 1997; Zhou et al., 1999). Another potential candidate for this function is the CD44-homolog LYVE-1, expressed in lymph and liver sinusoids as well as in peripheral lymphatics (Mouta Carreira et al., 2001). In fact, amongst the numerous HA receptors that have been proposed so far (encompassing CD44, RHAMM, layilin and TLR-2 and -4), it is unclear which ones are involved in HA internalization for degradation as compared to HA-mediated signal transduction.

The present study was designed with the objective of refining the model of HA catabolism in the mouse. For this purpose, we followed fluorescein-labeled HA (flHA) distribution after i.v. or s.c. administration in C57BL/6 mice in different body compartments potentially involved in HA turnover. We analyzed flHA size and distribution in skin, its uptake in lymph nodes, liver, spleen and kidney, and its pharmacokinetic parameters following i.v. administration. We found that a significant amount of flHA was locally converted to low molecular weight (MW) fragments in the skin, and that the remainder of the flHA at 4 days post-injection co-localized with F4/80-positive macrophages and LYVE-1-positive lymphatics, through which the molecule reached the lymph nodes where it was taken up by HARE-positive cells in medullary sinuses. In the vascular compartment, flHA displayed pharmacokinetic properties compatible with a Michaelis–Menten model of saturable receptor-mediated clearance, with a K_m of 11.6 μg/ml and a maximum elimination rate (V_{max}) of 1.69 μg/ml/min, which suggests that the system has a high HA clearance capacity and remains grossly linear above normal plasma HA concentration (~400 ng/ml in C57BL/6 mice). flHA is then removed from the blood by HARE-positive liver and spleen sinusoids. Taken together, these results are a step forward in the understanding of HA turnover for future studies.

2. Results

2.1. flHA labeling and functional characterization

Fluorescein was covalently attached to 1.2 MDa HA according to the published procedure (Mochizuki et al., 2009), resulting in a fluorescein/HA disaccharide ratio of ~0.02–0.03 as reported by the authors. Two different batches of flHA were used throughout this study.

In order to ensure that the resulting molecule remained a functional substrate for hyaluronidase degradation, it was incubated with recombinant human PH20 (rHuPH20) and the digestion was allowed to proceed overnight at neutral pH. This reaction also generated low MW flHA that were used as a control for the specificity of tissue uptake after i.v. administration (see below). HA degradation was assessed by agarose gel electrophoresis and size exclusion chromatography (Fig. 1A and B). flHA was detected in agarose gels using two different methods, direct fluorescence on an ultraviolet light transilluminator to detect the fluorescein, and Stains-All staining to visualize the HA backbone. Both signals overlapped, demonstrating that fluorescein and HA were part of the same molecule, and showed a shift in size from high MW (1.2 MDa; Fig. 1A and B, Lane 1) to lower MW flHA after incubation with rHuPH20 (Fig. 1A and B, Lane 3). Incubation of flHA overnight at 37 °C in PBS containing 0.1% BSA did not produce any significant shift in MW or decrease in signal intensity (Fig. 1A and B, Lane 2). Gel filtration chromatography similarly revealed a shift from high MW flHA, recovered in the void of the Zenix SEC-100 column (>700 kDa) to lower MW flHA (≤160 kDa; Fig. 1C). A complete digestion of flHA was not achieved in this case, likely due to the very low amount of rHuPH20 used in light of the fact that the digestion products would be injected in mice in subsequent experiments and that the impact of the enzyme needed to be minimized.

To further characterize flHA, binding was compared with unlabeled HA by competitive inhibition of biotin-labeled HA binding to HA binding protein (HABP)-coated wells (Supplementary Fig. 1). The binding of biotin-labeled HA to HABP was similarly inhibited by the presence of equivalent concentrations of HA or flHA.

Substrate suitability was examined by assessing depolymerization kinetics of unlabeled HA or flHA following incubation with increasing amounts of rHuPH20 (Supplementary Fig. 2). The MW of flHA after rHuPH20 incubation, as determined by agarose gel electrophoresis, was comparable to that of unlabeled HA for all enzyme concentrations.

From these results we concluded that flHA was recognized as a substrate by mammalian hyaluronidases and displayed similar binding and degradation kinetics compared to those of unlabeled HA. We therefore assumed that the exogenously administered flHA would be a relatively accurate reflection of endogenous HA catabolic pathways.

2.2. flHA is digested to low MW products in the skin

Following s.c. administration of 0.5 mg flHA in the thigh – a dose selected based upon the relative amounts of HA found in the skin (Reed et al., 1988) –, size exclusion chromatography of skin samples extracted at the site of injection revealed the progressive conversion of high MW material (eluting in the void of the column, >700 kDa) to lower MW species over time (<17 kDa, Fig. 2A–F). flHA signal intensity progressively decreased in corresponding cryosections of those samples. Whereas fluorescence was intense in cryosections

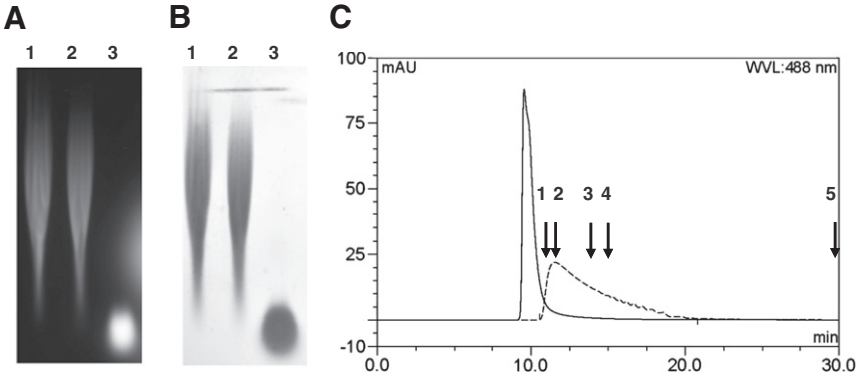

Fig. 1. Fluoresceinamine labeling of HA and hyaluronidase digestion. (A–B) Stains-all staining (A) and direct fluorescence visualization (B) of 1.2 MDa and rHuPH20 digested flHA run on a 0.5% agarose gel. Lane 1, 1.2 MDa flHA after labeling and purification; Lane 2, 1.2 MDa flHA incubated overnight at 37 °C in rHuPH20 digestion buffer (PBS, 0.1% BSA); Lane 3, flHA after overnight rHuPH20 digestion at 37 °C. (C) Gel filtration chromatography analysis of 1.2 MDa flHA (plain line) and rHuPH20-digested flHA (dashed line) at 488 nm on a Zenix SEC-100 column. 1, thyroglobulin (700 kDa); 2, gammaglobulin (160 kDa); 3, ovalbumin (44 kDa); 4, myoglobin (17 kDa); 5, vitamin B12 (1350 Da).

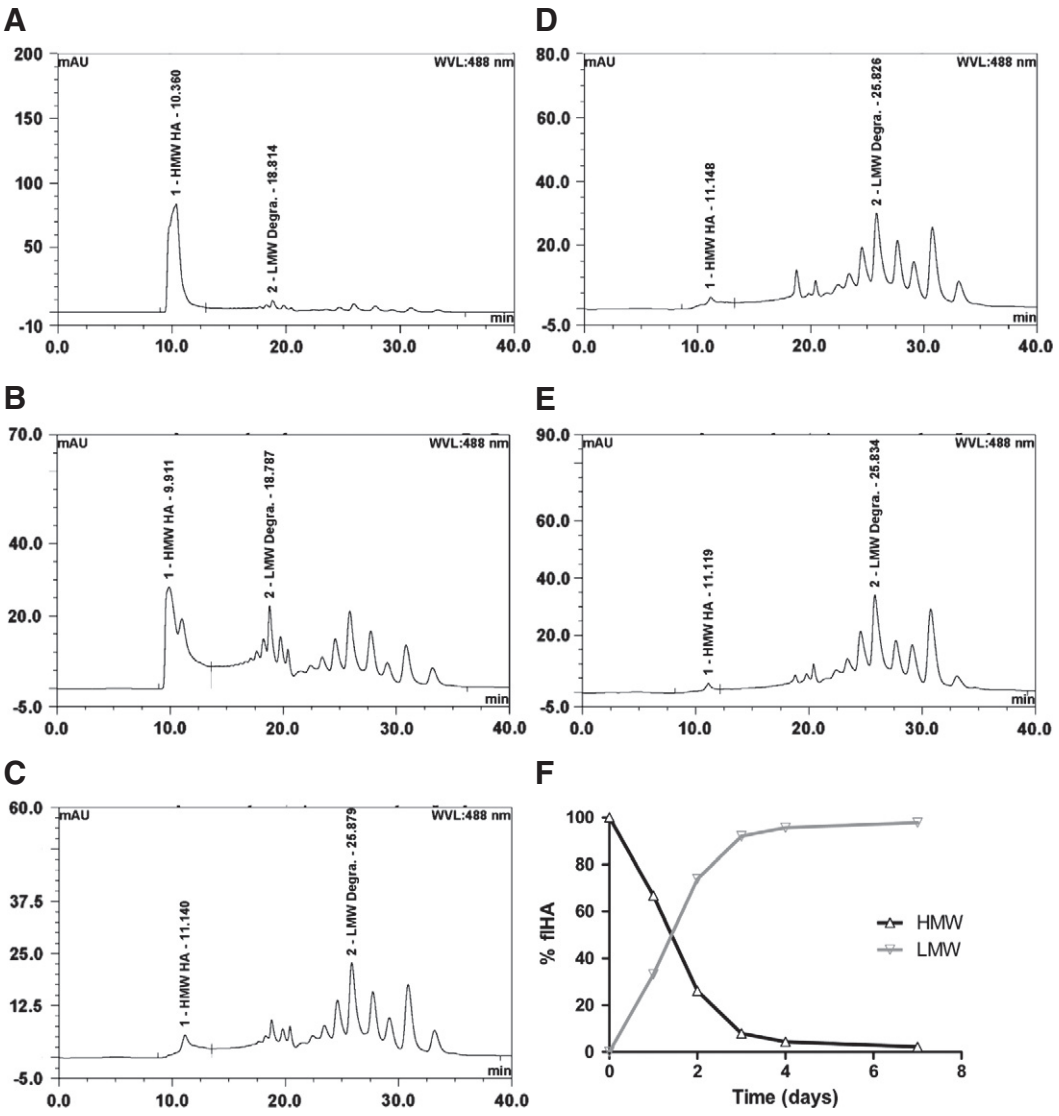

Fig. 2. flHA degradation in the skin. (A–E) Chromatograms showing the conversion of high MW to low MW flHA in mouse skin extracts of a representative subject at (A) 1 day, (B) 2 days, (C) 3 days, (D) 4 days and (E) 7 days after s.c. injection of 0.5 mg flHA in the thigh. 1, thyroglobulin (700 kDa); 2, gammaglobulin (160 kDa); 3, ovalbumin (44 kDa); 4, myoglobin (17 kDa); 5, vitamin B12 (1350 Da). (F) Proportion of high and low MW flHA in mouse skin extracts after s.c. injection of 0.5 mg flHA in the thigh over time. Values were calculated by comparing the AUC of the fluorescent peak recovered in the void or of all peaks eluted within the fractionation range of the Zenix SEC-100 column with the total AUC at 488 nm (n = 4).

obtained 1 day after injection (Fig. 3A), at 4 days post-injection most of the signal had disappeared from superficial skin layers, and the remainder appeared either associated with cells in the stroma, localized in sebaceous glands or lining the epidermis (Fig. 3B). Fluorescence intensity remained higher in the s.c. space, as compared to other skin layers. In order to identify the cell types or structures responsible for flHA uptake, co-localization experiments were attempted in one of the samples using antibodies recognizing CD31, F4/80, vimentin and LYVE-1 as markers of blood vessels, macrophages, fibroblasts and lymphatics, respectively, and CD44 and HARE as other major HA receptors. Three fields were viewed each time. flHA co-localized mainly with F4/80 and LYVE-1 in the s.c. space of skin cryosections, suggesting that both macrophages and lymphatics could be involved in its removal from the skin (Fig. 3C). HARE labeling was negative in the skin (data not shown).

2.3. flHA is taken up by medullary sinuses in the lymph nodes

After injection of 0.1–0.5 mg flHA in the s.c. space of the thigh, fluorescence was recovered in cryosections of the corresponding inguinal lymph node at all time points observed, i.e., 1–24 h (Fig. 4A). The signal was prominently found in HARE-positive medullary sinuses, as demonstrated by immunofluorescence labeling (Fig. 4B). It is worthy of note that a similar association was observed with LYVE-1, also expressed in lymph sinuses (data not shown).

A similar pattern of binding was observed after in vitro incubation of mouse lymph node sections with flHA and was inhibited by unlabeled HA (Supplementary Fig. 3A, left panels). Co-immunolabeling of CD44, HARE and LYVE-1 revealed a strong association of flHA with HARE-positive LYVE-1-positive sinusoidal cells (Supplementary Fig. 3B, left panels). Little colocalization was observed with CD44-positive cells.

2.4. flHA clearance from the blood is compatible with a Michaelis–Menten model of pharmacokinetics

After i.v. administration of several doses of flHA (1.4 μg, 10 μg, and 100 μg per mouse with an average weight of 21.36 ± 1.65 g [mean ± SD]), mouse plasma was collected at various time points and the fluorescence intensity was measured to determine flHA concentration

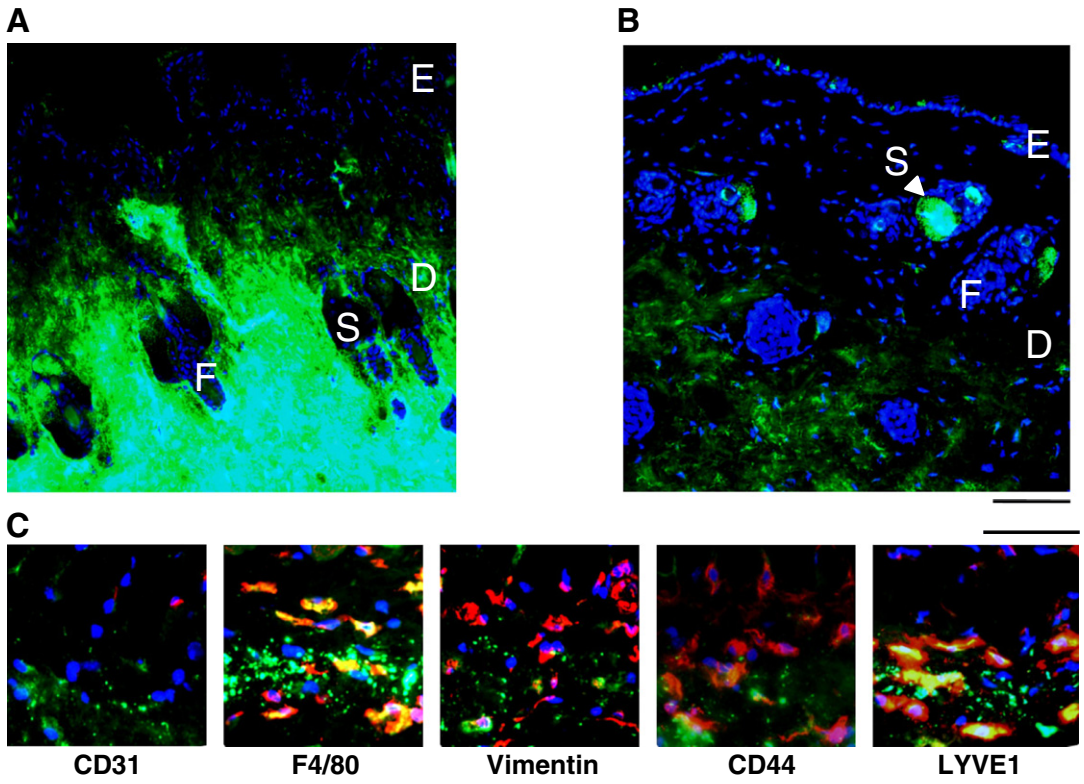

Fig. 3. flHA distribution in the skin. (A–B) Localization of flHA (green) in cryosections of mouse skin samples obtained (A) 1 day or (B) 4 days after s.c. injection of 0.5 mg flHA in the thigh (DAPI, blue; E, epidermis; D, dermis; F, hair follicle; S, sebaceous gland; magnification bar represents 150 μm; n = 4). (C) Co-immunolabeling of specific cell markers (red) in cryosections of a mouse skin sample at the 4 day time point demonstrating an association between flHA and F4/80 and LYVE-1-positive cells in the subcutis (colocalization, yellow; DAPI, blue; magnification bar represents 100 μm).

based on a 4-parameter standard curve obtained from standards of known concentration. Parameters of a one-compartment pharmacokinetic model with Michaelis–Menten elimination were fitted to the plasma concentration vs. time data collected from mice dosed with flHA. Estimates of Michaelis–Menten parameters K_m (11.6 μg/ml; 46.0% CV), V_{max} (1.69 μg/ml/min; 59.7% CV), and volume of distribution (V_d) (0.891 ml; 16.7% CV) are summarized in Table 1. Plasma concentration data are plotted together with simulations from fitted model parameters for each dose level in Fig. 5.

2.5. flHA is removed from plasma by sinusoidal cells of the liver and spleen

After i.v. injection of 5–100 μg flHA, most of the fluorescence signals were recovered in liver sinusoids and in the red pulp of the spleen (Fig. 6A). Only a low signal was observed in the kidney. Comparison of the distribution of a 100 μg dose of 1.2 MDa flHA to that of the same dose of hyaluronidase-digested low MW flHA revealed a dramatic decrease in signal intensity in all three tissues, demonstrating that the uptake of flHA is dependent on an HA structure-specific mechanism and is not an artifact due to the presence of the fluorochrome (Fig. 6A). Various immunolabelings were performed to characterize the cell populations responsible for flHA uptake. They included cell type-specific markers such as CD31 and F4/80 to label endothelial cells and macrophage/Kupffer cells respectively, as well as two HA receptors: CD44, present in Kuppfer cells, and HARE, expressed in liver and spleen sinusoids. Most of the fluorescence was associated with CD31-positive HARE-positive sinusoidal endothelial cells in the liver, with only a small proportion observable in association with F4/80-positive CD44-positive Kupffer cells (Fig. 6B). In the spleen, the fluorescence was also associated with HARE-positive sinusoidal cells (Fig. 6C).

Similar patterns were observed after in vitro incubation of mouse spleen and liver sections with flHA and were inhibited by co-incubation with unlabeled HA (Supplementary Fig. 3A, middle and right panels). Co-immunolabeling of CD44, HARE and LYVE1 revealed a strong association of flHA with HARE-positive LYVE-1-positive cells in the liver and HARE-positive cells in the spleen (Supplementary Fig. 3B, middle and right panels). Once again, little co-localization was observed with CD44-positive cells.

3. Discussion

In this study we sought to address HA catabolism in a mammalian system, specifically in the widely used C57BL/6 mouse model. The current hypothesis to describe HA degradation, proposed in 2001 (Csoka et al., 2001), is that HYAL1 and HYAL2 are the two major somatic hyaluronidases and act in concert to degrade HA, starting with HYAL2 at the plasma membrane generating intermediate MW fragments, then relayed by HYAL1 and exoglycosidases as those intermediate size fragments are subject to internalization by a receptor-mediated process to end up in the endosomal–lysosomal compartment.

From a more global perspective, HA catabolism appears to be strongly tissue-dependent and follows an ordered pathway involving specialized tissues such as the lymph node and liver, and specific HA receptors. Despite the availability of HYAL1- and HYAL2-deficient mouse models, little is known about the involvement of these hyaluronidases in this process. Early studies of systemic HA turnover led to the conclusion that HA catabolism in local tissues is probably not a major pathway for HA removal (Fraser et al., 1988; Reed et al., 1990a; Laurent et al., 1991). According to models generated from such studies, a significant proportion of HA is taken up by the lymphatic system to be extracted from the lymph by the lymph nodes.

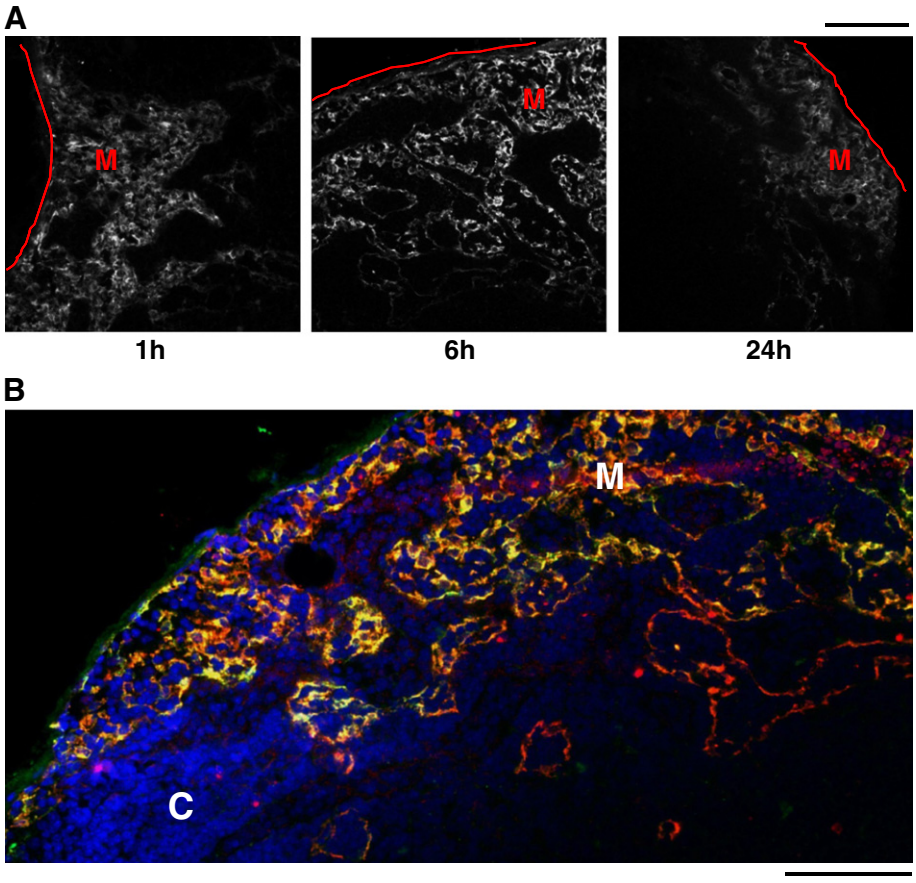

Fig. 4. flHA uptake in the lymphatic sinuses. (A) Distribution of flHA (green) in 7 μm cryosections of mouse inguinal lymph nodes obtained 1–24 h after s.c. injection of 0.1 mg flHA in the thigh (red line represents the edge of the lymph node; M, medullary sinuses; magnification bar represents 100 μm). (B) Colocalization of flHA (green) with HARE (red) in cryosections of mouse inguinal lymph node at the 6 h time point (colocalization, yellow; DAPI, blue; M, medullary sinuses; C, cortex; magnification bar represents 150 μm; n = 4–5).

The remainder (~10%) enters the bloodstream transiently via the thoracic duct to be rapidly metabolized by the liver. A more recent study suggests that lymphatic removal may have been overestimated and may be a minor component, with local hyaluronidase activity accounting for most of HA catabolism (Armstrong and Bell, 2002). In the present work, we examined skin as a representative local tissue and investigated lymph nodes, liver, spleen and kidney as potential sites of HA uptake and degradation. We chose to focus on two HA-receptors, CD44 and HARE, which are expressed in cell types that could participate in the clearance of HA and have largely been implicated in HA endocytosis (Zhou et al., 2000; Weigel and Weigel, 2003; Bourguignon et al., 2004; Harris et al., 2004; Harada and Takahashi, 2007). However, the present data show no functional evidence of CD44 or HARE-mediated HA internalization and cannot therefore rule out a possible contribution of other receptors (e.g., RHAMM, LYVE-1, layilin). For instance, LYVE-1 is expressed in sinusoidal cells of the lymph node and liver (Mouta Carreira et al., 2001, and data not shown) and could thus participate in HA uptake in those cells.

In order to follow HA uptake and catabolism in the organism, we generated a fluorescent, traceable HA molecule using a chemical reaction that results in the covalent attachment of fluoresceinamine to limited carboxyl groups of glucuronic acid residues of HA. To ensure that the modified molecule was still functional for binding and degradation, we used rHuPH20 to digest it to small size fragments.

Table 1
Michaelis–Menten pharmacokinetic parameters obtained with Phoenix WinNonlin®. K_m, Michaelis–Menten constant, V_d, volume of distribution, V_{max}, maximum metabolic rate, AUC, area under the curve, CV%, coefficient of variation.

Dose (ng)	K_m (ng/ml)	V_d (ml)	V_{max} (ng/ml/min)	AUC (min.ng/ml)	AUC CV%
1400	8250	0.958	1810	7230	6.81
10,000	17,700	0.721	2640	130,000	14.9
100,000	8730	0.994	627	9,470,000	11.9
Mean	11,600	0.891	1690		
CV%	46.0	16.7	59.7		

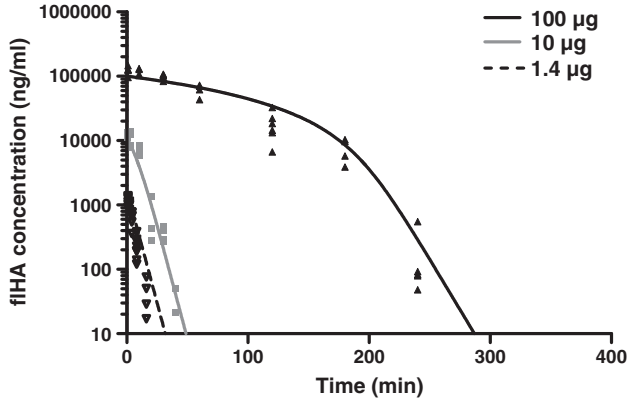

Fig. 5. Non-linear pharmacokinetic profile after i.v. injection of three different doses of flHA (1.4 μg, 10 μg, 100 μg) in the mouse described by a Michaelis–Menten model of saturable elimination. Symbols represent average concentrations from individual mice at each flHA dose, and, lines correspond to predicted curves based on Michaelis–Menten calculations (K_m = 11.6 μg/ml, V_{max} = 1.69 μg/ml/min, n = 5–8).

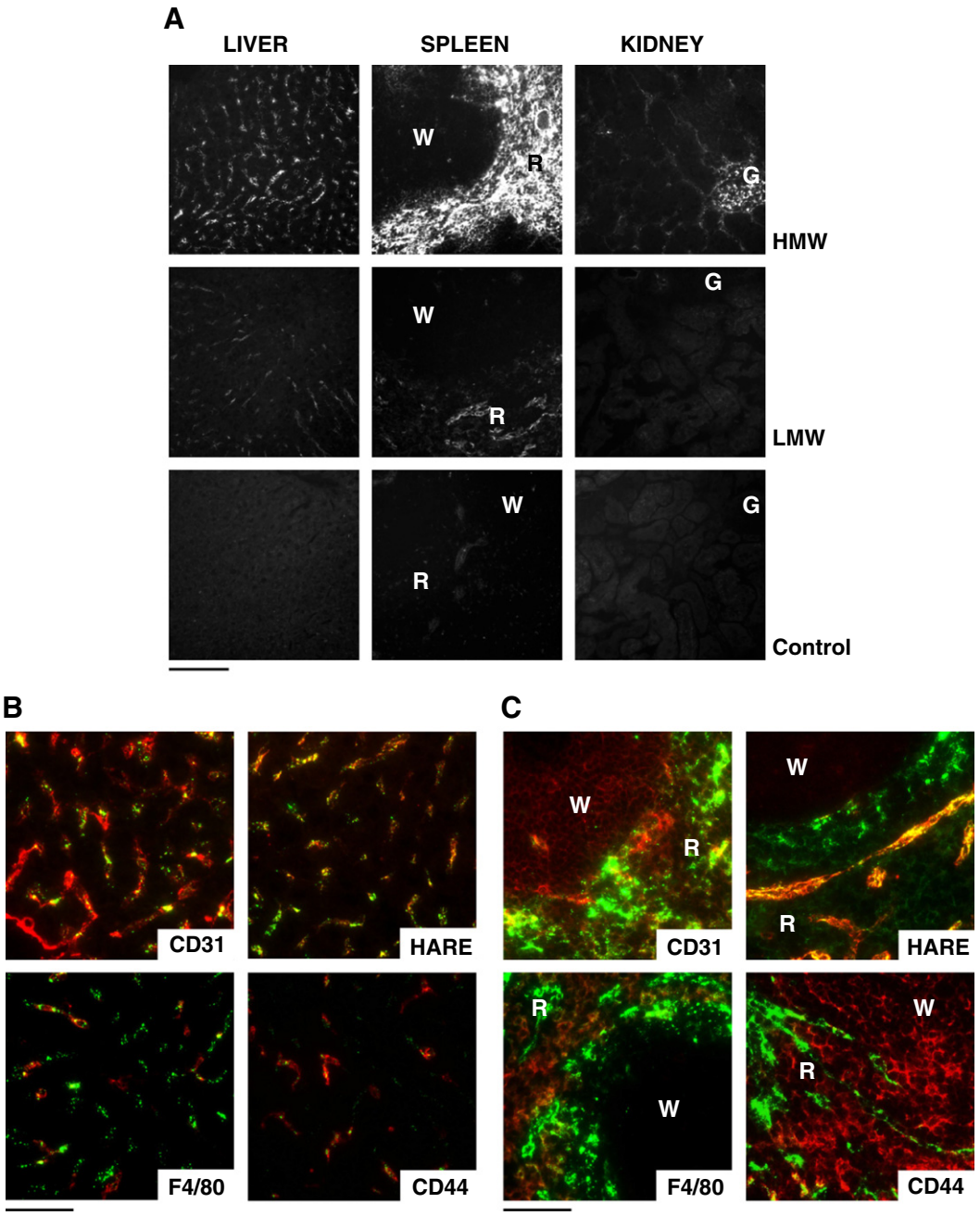

Fig. 6. flHA uptake in liver and spleen sinusoids. (A) Distribution of flHA in 7 μm cryosections of mouse liver, spleen and kidney samples obtained 10 min after i.v. injection of 0.1 mg flHA in a tail vein. (HMW, high molecular weight flHA; LMW, low molecular weight rHuPH20-digested flHA; control, saline; R, red pulp; W, white pulp; G, glomerulus; magnification bar represents 100 μm; n = 4–5). (B–C) Co-immunolabeling of flHA (green) with cell markers of endothelial cells (CD31, red) and of macrophages and Kupffer cells (F4/80, red) and two major HA receptors (HARE and CD44, red) in cryosections of mouse liver (B) and spleen (C) at 10 min post-injection of 0.1 mg flHA (DAPI, blue; R, red pulp; W, white pulp; G, glomerulus; magnification bar represents 50 μm, n = 4).

Interestingly, these low MW products were not taken up by the liver and spleen after i.v. administration. Due to their smaller size, we expect them to reach the urine through glomerular filtration in the kidneys, although we were unable to verify this hypothesis. Nevertheless, the size-dependence of flHA internalization allowed us to assume with confidence that the results obtained from our experiments could be attributed to an HA-specific structure and were not an artifact due to the presence of fluorescein on the HA backbone. The similar degradation and flHA binding compared to unlabeled HA in vitro, as well as the comparable binding patterns of flHA to mouse lymph node, spleen and liver sections in vivo and in vitro (in the latter case inhibited by unlabeled HA) all corroborate this conclusion.

Skin was selected as a tissue to study local HA catabolism due to its high HA concentration and turnover, and because it is an easily accessible organ for injection. It has been estimated that half of the total body HA resides in the skin (Reed et al., 1988) and is turned over with a half-life of less than a day (Reed et al., 1990a). In light of the high HA content of a human body (about 15 g), this suggests extremely active synthesis and degradation pathways.

S.c. injection in the thigh was preferred for delivery of a sufficient amount of flHA, and to achieve more consistent lymphatic drainage, limited to the inguinal lymph nodes. Gel filtration size exclusion chromatography analysis of skin samples collected at various time points after injection revealed the progressive appearance of low MW

species identified as flHA degradation products. The latter were recovered as several peaks with different retention times, allowing us to conclude that the replacement of high MW material (>700 kDa) by smaller molecules (<17 kDa) was due to a catalytic, enzyme-dependent mechanism generating intermediates rather than unspecific cleavage of fluorescein from the HA backbone.

From these results we conclude that local skin catabolism contributes to HA turnover. Degradation products could be detected one day after injection, but 4 days were needed for high MW polymers to completely disappear and only low MW degradation products (<17 kDa) to be detected. This coincided with the removal of most of the fluorescence from the different skin compartments as visualized in cryosections. The remainder, in the s.c. space, was mainly associated with F4/80- or LYVE-1-positive cells, most likely corresponding to macrophages and draining lymphatics. This suggests that HA can be degraded either locally or via the lymphatic system. It is also possible that after 4 days, some of the flHA had been catabolized and the degradation products cleared, including the fluorescein moieties, leading to underestimation of the local uptake by more active cell types. We chose not to quantify the proportion of remaining fluorescence in tissues relative to the initial dose in order to avoid artifacts due to the metabolism of the fluorescein label itself.

Other studies have proposed that endogenous HA in local tissues is constituted of two pools: a free pool that can be easily mobilized in case of increased lymph flow, and a less mobile pool corresponding for example to HA from cell-associated pericellular matrices (Laurent et al., 1991). The use of any exogenous HA should logically behave like the free pool and probably does not reflect the complete turnover of the immobilized pool, unless the latter simply results from HA-receptor interactions which can be competitively displaced by the exogenous HA.

Several studies, including the present one, suggest that HA can be catabolized within the lymphatic system (Fraser et al., 1988). For this reason, we examined local lymph nodes to assess their contribution to the uptake of flHA. Fluorescence was detected in cryosections of the lymphatic sinuses at all time points examined, i.e., as early as 1 h and as late as 24 h. In those samples, flHA was associated with HARE-positive cells. This receptor has been implicated in the removal of many waste products, such as glycation end products and possibly apoptotic cells (Tamura et al., 2003; Park et al., 2008), and was initially identified as an endocytic HA receptor (Zhou et al., 2003). Another candidate for HA uptake in the lymph nodes and liver is LYVE-1, a homolog of the CD44 HA receptor expressed in lymph and liver endothelia that binds and internalizes HA when transfected into cell cultures (Prevo et al., 2001). The individual contribution of these receptors has not been established and the possibility exists that they may be functionally redundant.

The remainder of HA, transported by the efferent lymph, enters the circulatory system via the thoracic duct. The concentration of HA is much lower in plasma than in lymph (Engstrom-Laurent et al., 1985; Reed et al., 1990b), probably as a result of very efficient clearance systems as demonstrated by its rapid turnover. We thus attempted to characterize HA turnover and pharmacokinetic properties in the bloodstream. Three major organs were examined: liver, considered the main site of HA uptake, spleen and kidneys.

Indeed, most of the i.v. administered flHA was detected in sinusoidal spaces of the liver and in the red pulp of the spleen, with a much fainter and inconsistent signal observed in the kidney. This is consistent with a whole body autoradiographic study performed in the mouse (Fraser et al., 1983). In the liver, flHA was largely co-distributed with CD31 and HARE, demonstrating that, in this tissue, liver sinusoidal endothelial cells are the main cells responsible for the uptake of flHA and, by extrapolation, of endogenous plasma HA, as has been suggested previously (Smedsrod et al., 1984; Fraser et al., 1985). This is in line with the proposed role of liver sinusoidal endothelial cells in the removal of many other compounds as part of the reticulo-endothelial system (Elvevold et al., 2008). In the spleen, some of the fluorescence was strongly associated with HARE-positive cells that most likely represent sinusoidal cells.

These studies support a model whereby HA is removed from plasma primarily by the liver and spleen, although the precise contribution of each organ is not known. Even if flHA deposits in the spleen were high, the liver could still be the major organ for blood removal of HA, based solely on the relative size of these two organs.

The measurement of fluorescence intensity in plasma samples collected at various time points after i.v. administration of several doses of flHA revealed non-linear pharmacokinetics that could be fitted to a Michaelis–Menten model, consistent with a saturable receptor-mediated clearance mechanism. Such saturable pharmacokinetics were reported in sheep using radiolabeled HA (Lebel et al., 1989), and in humans for HA administered in healthy volunteers (Hamilton et al., 2009). The first study, however, reported K_m and V_{max} values in sheep that were much lower than values calculated from our study, i.e., 0.12 μg/ml and 62 ng/ml/min (3.32 μg/kg/min) respectively, as compared to 11.6 μg/ml and ~75 μg/kg/min in the present work. By contrast, the study conducted by Hamilton and colleagues in humans, reports a V_{max} of 348 mg/kg/h (5.8 mg/kg/min) and a K_m between 6.4 and 26.5 mg/ml, both values much higher than what we found in this study. This suggests that the kinetics of HA turnover may differ between species.

However, the turnover of circulating HA in the mouse, calculated based on the present data, falls within a similar range to what has been estimated for humans. For instance, considering a mean steady state plasma HA concentration of 400 ng/ml in the C57BL/6 mouse, the plasma elimination rate, equal to the HA input in homeostatic conditions, is in the order of 50 ng/min according to the Michaelis–Menten equation, with a calculated half-life of ~5 min, comparable to what has been described in the literature for humans, i.e., 2–5 min (Fraser et al., 1981). A possible explanation for these observations is that basal catabolism of HA is grossly similar among species, but differs upon saturation of the system, possibly due to interspecies differences in receptor affinities or receptor and degrading enzyme expression levels. Results may also vary with the size of HA used for the studies, which may impact its uptake in tissues (Mochizuki et al., 2009).

In summary, the present work provides a framework to characterize HA clearance in the mouse, a model that is widely used in exploratory and preclinical research. According to our results, HA is partially catabolized in local tissues, but can also be taken up in the lymph nodes. While very little local HA reaches the bloodstream, its removal from the vascular compartment is rapid and mediated by the liver and spleen sinusoids, probably through receptor-mediated endocytosis and according to Michaelis–Menten pharmacokinetics. This first comprehensive analysis of systemic HA turnover in the mouse uses fluorescence detection methods to track exogenously administered fluorescein-labeled HA very precisely. From a global perspective, this provides us with a basic understanding of HA turnover in physiological conditions and in a normal organism as a prerequisite for further, pathophysiology-oriented studies on perturbations of the catabolic pathways of HA.

4. Experimental procedures

4.1. Mice

C57BL/6 mice (Taconic Farms, New York, NY) were used in this study. All experimental procedures on animals were conducted in compliance with the National Research Council's “Guide for the Care and Use of Laboratory Animals” and followed detailed written protocols that were approved by the Institutional Animal Care and Use Committee (IACUC).

4.2. HA-fluoresceinamine conjugation

HA of bacterial origin was labeled with fluoresceinamine using a modified version of the method described by de Belder and Wik (1975) and adapted by Mochizuki et al. (2009). Briefly, 100 mg of HA (1.2 MDa, medical grade, <0.02 EU/mg endotoxin; Lifecore, Chaska, MN) was dissolved in 80 ml ddH_2O and 40 ml DMSO. Fifty mg of fluoresceinamine, isomer 1 (Sigma, St. Louis, MO), 50 µl acetaldehyde and 50 µl cyclohexyl isocyanide (Sigma) were dissolved in 0.9 ml DMSO and added to the HA solution. The reaction was allowed to proceed for 5 h at room temperature in the dark with mild agitation, followed by overnight precipitation of the labeled HA with 14 volumes of ethanol and 7.75 ml of 6 M guanidine-hydrochloride per 10 ml of reaction mixture. The material was recovered by centrifugation at 2000 g and resuspended in ddH_2O at 4 °C overnight, then extensively dialyzed against ddH_20 using Snake Skin 10,000 MWCO membranes (ThermoScientific, Rockford, IL), aliquoted and stored at −80 °C.

4.3. Hyaluronidase digestion of flHA

flHA at a concentration of 1 mg/ml was incubated overnight with 100 ng/ml rHuPH20 (Bookbinder et al., 2006) in PBS (pH7.3) containing 0.1% BSA at 37 °C. rHuPH20 was omitted in the control sample. Sixteen µg of each reaction product was diluted in loading buffer (12% w/v glycerol in TAE) and run on a 0.5% agarose gel in TAE buffer for 5 h at 60 V. The gel was visualized on an ultraviolet light transilluminator, briefly rinsed in distilled water and stained overnight in 50% ethanol containing 0.005% w/v Stains-All (Sigma), then observed on a white light transilluminator. The samples were also analyzed by gel filtration high performance liquid chromatography on a Sepax Zenix® SEC-100 column (Sepax Technologies, Newark, DE) equilibrated with 300 mM phosphate buffer, pH 7, as a second method to characterize the size distribution of the flHA products.

4.4. In vivo experiments

flHA was administered into mice either i.v. in a tail vein or s.c. in the thigh. At selected time points, exsanguination was performed under isoflurane anesthesia, followed by cervical dislocation. Blood, collected in EDTA-coated vials, was kept on ice and centrifuged at 3000 rpm for 10 min in a tabletop centrifuge to obtain plasma. In some cases, tissue samples were harvested and frozen in Tissue-Tek OCT compound (Sakura, Zoeterwoude, The Netherlands) on dry-ice cooled methylbutane for subsequent histological examination, or in liquid nitrogen for chromatography analysis of flHA content.

4.5. Analysis of flHA size distribution by chromatography

Skin samples were minced with a pair of scissors before addition of 4 volumes of lysis buffer (250 mM phosphate buffer, 500 mM NaCl, pH7, 1% Tween20, 0.02% sodium azide) and incubated for ~30 h at 4 °C on a rotating wheel according to the procedure described by Laurent et al. (1991). Samples were then centrifuged for 1 min at 14,000 rpm to remove debris, then 45 min at 14,000 rpm at 4 °C. The supernatant was filtered through a Costar® 0.45 µm microspin filter (Corning, Lowell, MA) and loaded on a Zenix® SEC-100 column (Sepax) equilibrated with 300 mM phosphate buffer, pH 7. A cutoff size was manually applied to differentiate between high MW (eluting in the void of the column) and low MW flHA and the AUC was measured for both species to determine their proportions as a percentage of the overall fluorescence.

To evaluate the efficiency of this extraction method, two skin samples (Sample A, 1 day post-s.c. injection of 0.5 mg flHA, and Sample B, 7 days post-s.c. injection of 0.5 mg flHA) were subjected to two successive overnight extractions in 4 volumes of the above-mentioned buffer, followed by a third extraction in 8 volumes of 4 M guanidine-HCl. Extracts were analyzed by gel filtration chromatography on a Zenix-SEC 100 column (Sepax), and the AUC of the fluorescence at 488 nm measured. The proportion of fluorescence in each extract was expressed as a percentage of the total fluorescence for each sample (Supplementary Table 1).

4.6. Antibodies, immunolocalization and microscopy

Tissue samples were cryosectioned using a CM3000 cryostat (Leica Microsystems, Wetzlar, Germany) into 7 µm-thick sections. Sections were air-dried and stored at −80 °C until further processing. Slides were fixed in ethanol:acetone 25:75 for 10 min at −20 °C and air-dried again, then washed in PBS before being either directly coverslipped using ProLong® Gold antifade reagent with DAPI (Invitrogen, Carlsbad, CA) or processed for immunolabeling. Rat monoclonal anti-CD44 and anti-CD31 (BD, Franklin Lakes, NJ; Cat. 550538 and 550274), rabbit polyclonal anti-vimentin antibody (Abcam, Cambridge, MA; Cat. ab45939) and goat polyclonal anti-HARE (Santa Cruz Biotechnology, Santa Cruz, CA; Cat. sc27752) were used at a 1:50 dilution. Rat monoclonal anti-F4/80 (Fitzgerald, North Acton, MA; Cat. 10R-F100A) was used at a 1:100 dilution. Rabbit polyclonal anti-LYVE1 (Abcam, Cat. ab14917) was used at a 1:1000 dilution. Secondary antibodies were Alexa Fluor® 594-conjugated anti-rat, anti-rabbit or anti-goat immunoglobulins (Invitrogen) used at a 1:500 dilution. Sections were blocked for 1 h at room temperature in 5% goat serum in PBS (for rat and rabbit primary antibodies) or 5% donkey serum in PBS (for goat primary antibodies), then incubated either overnight at 4 °C or for 2 h at room temperature with the primary antibodies. Slides were washed in PBS-0.05% Tween-20 and incubated with secondary antibodies for 45 min at room temperature, then washed again in PBS-0.05% Tween-20 and coverslipped using ProLong® Gold antifade reagent with DAPI (Invitrogen). Tissue sections were observed under a Zeiss Axioskop microscope (Zeiss, Oberkochen, Germany) or an inverted Eclipse TE2000-U microscope (Nikon, Tokyo, Japan), both equipped with a Lumen200 light source (Prior Scientific, Rockland, MA), and micrographs were captured using an RT3 or a Pursuit camera (Spot Imaging Solutions, Diagnostic Instruments, Sterling Heights, MI).

4.7. Fluorescence intensity measurements

Fluorescence in plasma samples, either undiluted or diluted with PBS or mouse plasma, was measured using a multi-well plate spectrofluorimeter (SpectraMax M2, Molecular devices, Sunnyvale, CA), set on an excitation wavelength of 490 nm and an emission wavelength of 520 nm. flHA standards were prepared to translate fluorescence values into flHA concentrations based on a 4-parameter standard curve calculated using Softmax Pro 5.3 (Molecular Devices).

4.8. Pharmacokinetic analysis

Phoenix® WinNonlin® 6.1 (Pharsight, St. Louis, MO) was used for pharmacokinetic analysis of plasma flHA versus time data. For calculations, values that fell below the quantitation limit (<15 ng/ml) were not included in the analysis and nominal time points were used. Plasma concentration data were used to estimate Michaelis–Menten model parameters assuming a one-compartment i.v. bolus input (Model 301). Parameters included V_d (ml), V_{max} (ng/ml/min), and K_m (Michaelis–Menten constant (ng/ml) of injected flHA. The plasma flHA concentration (C) after i.v. administration was described by the equation $dC/dt = -V_{max}.C/(K_m + C)$ where $C_{(0)} = Dose/V_d$.

Acknowledgments

We would like to acknowledge H. Michael Shepard and Bruno Flamion for scientific discussions, Li Zhu for technical help, Alex Oh and Dan Maneval for the pharmacokinetic analyses and the preclinical staff of Halozyme Therapeutics for husbandry and in vivo support.

Appendix A. Supplementary data

Supplementary data to this article can be found online at doi:10.1016/j.matbio.2011.11.002.

References

Armstrong, S.E., Bell, D.R., 2002. Relationship between lymph and tissue hyaluronan in skin and skeletal muscle. Am. J. Physiol. Heart Circ. Physiol. 283, H2485–H2494.
Bookbinder, L.H., Hofer, A., Haller, M.F., Zepeda, M.L., Keller, G.A., Lim, J.E., Edgington, T.S., Shepard, H.M., Patton, J.S., Frost, G.I., 2006. A recombinant human enzyme for enhanced interstitial transport of therapeutics. J. Control. Release 114, 230–241.
Bourguignon, L.Y., Singleton, P.A., Diedrich, F., Stern, R., Gilad, E., 2004. CD44 interaction with Na^+-H^+ exchanger (NHE1) creates acidic microenvironments leading to hyaluronidase-2 and cathepsin B activation and breast tumor cell invasion. J. Biol. Chem. 279, 26991–27007.
Csoka, A.B., Scherer, S.W., Stern, R., 1999. Expression analysis of six paralogous human hyaluronidase genes clustered on chromosomes 3p21 and 7q31. Genomics 60, 356–361.
Csoka, A.B., Frost, G.I., Stern, R., 2001. The six hyaluronidase-like genes in the human and mouse genomes. Matrix Biol. 20, 499–508.
de Belder, A.N., Wik, K.O., 1975. Preparation and properties of fluorescein-labelled hyaluronate. Carbohydr. Res. 44, 251–257.
DeAngelis, P.L., Weigel, P.H., 1994. Immunochemical confirmation of the primary structure of streptococcal hyaluronan synthase and synthesis of high molecular weight product by the recombinant enzyme. Biochemistry 33, 9033–9039.
DeAngelis, P.L., Papaconstantinou, J., Weigel, P.H., 1993. Molecular cloning, identification, and sequence of the hyaluronan synthase gene from group a streptococcus pyogenes. J. Biol. Chem. 268, 19181–19184.
Duran-Reynals, F., 1928. Exaltation de l'activite du virus vaccinal par les extraits de certains organes. CR Séances Soc. Biol. Fil. 99, 6–7.
Elvevold, K., Smedsrod, B., Martinez, I., 2008. The liver sinusoidal endothelial cell: a cell type of controversial and confusing identity. Am. J. Physiol. Gastrointest. Liver Physiol. 294, G391–G400.
Engstrom-Laurent, A., Laurent, U.B., Lilja, K., Laurent, T.C., 1985. Concentration of sodium hyaluronate in serum. Scand. J. Clin. Lab. Invest. 45, 497–504.
Fraser, J.R., Laurent, T.C., Pertoft, H., Baxter, E., 1981. Plasma clearance, tissue distribution and metabolism of hyaluronic acid injected intravenously in the rabbit. Biochem. J. 200, 415–424.
Fraser, J.R., Appelgren, L.E., Laurent, T.C., 1983. Tissue uptake of circulating hyaluronic acid. A whole body autoradiographic study. Cell Tissue Res. 233, 285–293.
Fraser, J.R., Alcorn, D., Laurent, T.C., Robinson, A.D., Ryan, G.B., 1985. Uptake of circulating hyaluronic acid by the rat liver. Cellular localization in situ. Cell Tissue Res. 242, 505–510.
Fraser, J.R., Kimpton, W.G., Laurent, T.C., Cahill, R.N., Vakakis, N., 1988. Uptake and degradation of hyaluronan in lymphatic tissue. Biochem. J. 256, 153–158.
Frost, G.I., Csoka, A.B., Wong, T., Stern, R., 1997. Purification, cloning, and expression of human plasma hyaluronidase. Biochem. Biophys. Res. Commun. 236, 10–15.
Hamilton, S.R., Veiseh, M., Tolg, C., Tirona, R., Richardson, J., Brown, R., Gonzalez, M., Vanzieleghem, M., Anderson, P., Asculai, S., Winnik, F., Savani, R., Freeman, D., Luyt, L., Koropatnick, J., Turley, E.A., 2009. Pharmacokinetics and pharmacodynamics of hyaluronan infused into healthy human volunteers. Open Drug Metab. J. 3, 43–55.
Harada, H., Takahashi, M., 2007. CD44-dependent intracellular and extracellular catabolism of hyaluronic acid by hyaluronidase-1 and -2. J. Biol. Chem. 282, 5597–5607.
Harris, E.N., Weigel, J.A., Weigel, P.H., 2004. Endocytic function, glycosaminoglycan specificity, and antibody sensitivity of the recombinant human 190-kDa hyaluronan receptor for endocytosis (HARE). J. Biol. Chem. 279, 36201–36209.
Itano, N., Kimata, K., 1996a. Molecular cloning of human hyaluronan synthase. Biochem. Biophys. Res. Commun. 222, 816–820.
Itano, N., Kimata, K., 1996b. Expression cloning and molecular characterization of has protein, a eukaryotic hyaluronan synthase. J. Biol. Chem. 271, 9875–9878.
Itano, N., Sawai, T., Yoshida, M., Lenas, P., Yamada, Y., Imagawa, M., Shinomura, T., Hamaguchi, M., Yoshida, Y., Ohnuki, Y., Miyauchi, S., Spicer, A.P., McDonald, J.A., Kimata, K., 1999. Three isoforms of mammalian hyaluronan synthases have distinct enzymatic properties. J. Biol. Chem. 274, 25085–25092.
Laurent, U.B., Dahl, L.B., Reed, R.K., 1991. Catabolism of hyaluronan in rabbit skin takes place locally, in lymph nodes and liver. Exp. Physiol. 76, 695–703.
Lebel, L., Fraser, J.R., Kimpton, W.S., Gabrielsson, J., Gerdin, B., Laurent, T.C., 1989. A pharmacokinetic model of intravenously administered hyaluronan in sheep. Pharm. Res. 6, 677–682.
Markovitz, A., Cifonelli, J.A., Dorfman, A., 1958. Biosynthesis of hyaluronic acid by cell-free extracts of group —a streptococci. Biochim. Biophys. Acta 28, 453–455.
Mochizuki, S., Kano, A., Shimada, N., Maruyama, A., 2009. Uptake of enzymatically-digested hyaluronan by liver endothelial cells in vivo and in vitro. J. Biomater. Sci. Polym. Ed. 20, 83–97.
Mouta Carreira, C., Nasser, S.M., di Tomaso, E., Padera, T.P., Boucher, Y., Tomarev, S.I., Jain, R.K., 2001. LYVE-1 is not restricted to the lymph vessels: expression in normal liver blood sinusoids and down-regulation in human liver cancer and cirrhosis. Cancer Res. 61, 8079–8084.
Park, S.Y., Jung, M.Y., Kim, H.J., Lee, S.J., Kim, S.Y., Lee, B.H., Kwon, T.H., Park, R.W., Kim, I.S., 2008. Rapid cell corpse clearance by stabilin-2, a membrane phosphatidylserine receptor. Cell Death Differ. 15, 192–201.
Prevo, R., Banerji, S., Ferguson, D.J., Clasper, S., Jackson, D.G., 2001. Mouse LYVE-1 is an endocytic receptor for hyaluronan in lymphatic endothelium. J. Biol. Chem. 276, 19420–19430.
Reed, R.K., Lilja, K., Laurent, T.C., 1988. Hyaluronan in the rat with special reference to the skin. Acta Physiol. Scand. 134, 405–411.
Reed, R.K., Laurent, U.B., Fraser, J.R., Laurent, T.C., 1990a. Removal rate of [3h]hyaluronan injected subcutaneously in rabbits. Am. J. Physiol. 259, H532–H535.
Reed, R.K., Laurent, T.C., Taylor, A.E., 1990b. Hyaluronan in prenodal lymph from skin: changes with lymph flow. Am. J. Physiol. 259, H1097–H1100.
Smedsrod, B., Pertoft, H., Eriksson, S., Fraser, J.R., Laurent, T.C., 1984. Studies in vitro on the uptake and degradation of sodium hyaluronate in rat liver endothelial cells. Biochem. J. 223, 617–626.
Smedsrod, B., Pertoft, H., Gustafson, S., Laurent, T.C., 1990. Scavenger functions of the liver endothelial cell. Biochem. J. 266, 313–327.
Spicer, A.P., Olson, J.S., McDonald, J.A., 1997. Molecular cloning and characterization of a cDNA encoding the third putative mammalian hyaluronan synthase. J. Biol. Chem. 272, 8957–8961.
Stern, R., 2003. Devising a pathway for hyaluronan catabolism: are we there yet? Glycobiology 13 (12), 105R–115R.
Stern, R., 2004. Hyaluronan catabolism: a new metabolic pathway. Eur. J. Cell Biol. 83, 317–325.
Strobl, B., Wechselberger, C., Beier, D.R., Lepperdinger, G., 1998. Structural organization and chromosomal localization of Hyal2, a gene encoding a lysosomal hyaluronidase. Genomics 53, 214–219.
Tamura, Y., Adachi, H., Osuga, J., Ohashi, K., Yahagi, N., Sekiya, M., Okazaki, H., Tomita, S., Lizuka, Y., Shimano, H., Nagai, R., Kimura, S., Tsujimoto, M., Ishibashi, S., 2003. Feel-1 and feel-2 are endocytic receptors for advanced glycation end products. J. Biol. Chem. 278, 12613–12617.
Watanabe, K., Yamaguchi, Y., 1996. Molecular identification of a putative human hyaluronan synthase. J. Biol. Chem. 271, 22945–22948.
Weigel, J.A., Weigel, P.H., 2003. Characterization of the recombinant rat 175-kDa hyaluronan receptor for endocytosis (HARE). J. Biol. Chem. 278, 42802–42811.
Yannariello-Brown, J., Zhou, B., Weigel, P.H., 1997. Identification of a 175 kDa protein as the ligand-binding subunit of the rat liver sinusoidal endothelial cell hyaluronan receptor. Glycobiology 7, 15–21.
Zhou, B., Oka, J.A., Singh, A., Weigel, P.H., 1999. Purification and subunit characterization of the rat liver endocytic hyaluronan receptor. J. Biol. Chem. 274, 33831–33834.
Zhou, B., Weigel, J.A., Fauss, L., Weigel, P.H., 2000. Identification of the hyaluronan receptor for endocytosis (HARE). J. Biol. Chem. 275, 37733–37741.
Zhou, B., McGary, C.T., Weigel, J.A., Saxena, A., Weigel, P.H., 2003. Purification and molecular identification of the human hyaluronan receptor for endocytosis. Glycobiology 13, 339–349.